

**UNIVERSIDADE DE SÃO PAULO**

**INSTITUTO DE FÍSICA  
CAIXA POSTAL 66318  
05389-970 SÃO PAULO - SP  
BRASIL**

# **PUBLICAÇÕES**

**IFUSP/P-1272**

**MEASUREMENTS OF DISCRETE AND CONTINUOUS  
X-RAY SPECTRA WITH A PHOTODIODE AT ROOM  
TEMPERATURE**

**X-RAY SPECTRAL MEASUREMENTS WITH A  
PHOTODIODE**

**Ricardo A. Terini<sup>1</sup>, Paulo R. Costa<sup>2</sup>, Tânia A.C. Furquim<sup>2</sup> and  
Silvio B. Herdade<sup>3</sup>**

<sup>1</sup>Departamento de Física - Pontifícia Universidade Católica de  
São Paulo.  
R. Marquês de Paranaguá, 111, 01303-050, São Paulo, SP-Brazil

<sup>2</sup>Instituto de Eletrotécnica e Energia- Universidade de São Paulo  
Av. Prof. Luciano Gualberto, 1289, 05508-900, São Paulo, SP-Brazil

<sup>3</sup>Instituto de Física, Universidade de São Paulo

Maio/1997

*Pag. 1-31*

# MEASUREMENTS OF DISCRETE AND CONTINUOUS X-RAY SPECTRA WITH A PHOTODIODE AT ROOM TEMPERATURE

## X-RAY SPECTRAL MEASUREMENTS WITH A PHOTODIODE

Ricardo A. Terini<sup>1</sup>, Paulo R. Costa<sup>2</sup>,  
Tânia A.C. Furquim<sup>2</sup> and Silvio B. Herdade<sup>3</sup>

<sup>1</sup> Departamento de Física - Pontifícia Universidade Católica de São Paulo  
R. Marquês de Paranaguá, 111, 01303-050, São Paulo, SP - Brazil.

<sup>2</sup> Instituto de Eletrotécnica e Energia - Universidade de São Paulo,  
Av. Prof. Luciano Gualberto, 1289, 05508-900, São Paulo, SP - Brazil.

<sup>3</sup> Instituto de Física - Universidade de São Paulo,  
Caixa Postal 66318, 05389-970, São Paulo, SP - Brazil

Address for correspondence:

Ricardo A. Terini

Departamento de Física - PUC - SP

R. Marquês de Paranaguá, 111, 01303-050, São Paulo, SP - Brazil.

FAX 55 011 256-5039, e-mail: rterini@exatas.pucsp.br.

## Abstract

Spectra of  $X$ - and  $\gamma$ -rays emitted by radioactive sources and of the radiation emitted by  $X$ -ray tubes, in the energy range 15–160 keV, have been measured with a silicon PIN photodiode at room temperature. The experimental  $X$ -ray tube spectra are compared with calculated ones on the basis of a semi-empirical model. Results indicate that the method utilized is adequate for the characterization of  $X$ -ray beams in the medical diagnostic energy region.

## Introduction

Silicon PIN photodiodes, in nuclear spectroscopic measurements, are mainly used for the detection of light from scintillators (Suffert, 1992). This combination offers several advantages as compared to photomultiplier tube-scintillator assembly as large quantum efficiency, no gain drifts in magnetic fields, low operating voltages and power consumption, as well as low cost. In direct measurements of  $X$ - and  $\gamma$ -rays, silicon PIN photodiodes have been also utilized, due to their extremely low leakage currents (down to few  $nA$ ) and low noise. As a semiconductor device, being 3.6 eV the average energy needed to create an electron-hole pair in the depletion layer, a great number of charge carriers are produced in a small volume by the ionizing radiation, reducing the statistical contribution to the peak-widths of energy spectra. PIN photodiodes with low capacitance even with large areas are now available, and their energy resolution have been reduced in the last ten years with the use of special designed devices and preamplifiers, as well as by cooling. Photodiodes with small active areas present a resolution of 1.2–2.0 keV at room temperature (Aoki and Koyama, 1989; Yamamoto et al, 1989; Ahmad et al, 1990; Gramsch et al, 1992) measured by the peak's full width

at half maximum (FWHM). This resolution can be compared to that of cooled Si(Li) detectors coupled to preamplifiers with cooled FET, which is in the range 0.6–0.8 keV (Ahmad and Wagner, 1974). Therefore, PIN photodiodes become competitive even for high resolution photon spectroscopy in the keV energy region.

On the other hand, the knowledge of the X-ray spectra is very important in many applications as, for example, in medical diagnostic radiology and in radiation dosimetry. This knowledge leads to patient dose reduction in radiological examinations and to optimize image quality in image receptors (Aoki and Koyama, 1989; Seelentag and Panzer, 1979; Pani et al, 1987). The characterization of a X-ray beam is also important to achieve spectral conformance with radiation emitters of different laboratories and to allow intercomparison of test results.

Measurements of medical diagnostic X-ray spectra have been reported by several authors, using different detectors: NaI(Tl) (Epp and Weiss, 1966), Ge(Li) or Si(Li) (Seelentag and Panzer, 1979; Israel et al 1971; Fewell and Shuping, 1977; O'Foghludha and Johnson, 1981), and surface barrier detectors (Pani et al, 1987). A comparison reveals large difference amongst the spectra obtained with such detectors. Ge or Si (Li) have been more frequently used for accurate spectral measurements, with proper corrections (Seelentag and Panzer, 1979; Fewell and Shuping, 1977). However, there are some disadvantages in using these systems: in measurements with medical X-ray equipment, it is necessary to decrease the count rate by using a pinhole collimator and to reduce the leakage current of the detector by cooling. With this collimation it is impossible to measure photons with different incident angles simultaneously, and hence, scattered radiation. Furthermore, the large liquid nitrogen container is inconvenient for certain applications, and there are an additional difficulty of working with high voltages.

Recently, a few papers have reported the use of PIN photodiodes for spectrometry of diagnostic X-rays (Aoki and Koyama, 1989; 1990). These devices combines low operating voltages, low leakage current and attractive cost, with good resolution even at room temperature, mainly for those with small junction areas. Thus, X-ray spectra can be measured without cooling when one doesn't wish extremely high resolution, which is the case in some applications. Although the detection efficiency for X-rays is extremely limited, this characteristic makes it possible to measure incident X-ray spectra without pinhole collimators. Due to their small dimensions, most of commercial PIN photodiodes can be easily utilized in measurements of primary radiation or inside phantoms.

This paper present some new measurements of discrete and continuous photon spectra, in the energy range 15–160 keV, with a photodiode at room temperature. The raw data are corrected by means of a stripping procedure which takes into account the photodiode full-energy absorption efficiency as a function of photon energy. Measured spectra of X-ray equipments are compared with spectra calculated on the basis of a semi-empirical model - the TBC model (Tucker, Barnes and Chakraborty, 1991).

### Experimental Method

The detector used for X-ray measurements was a Siemens SFH 206 K silicon planar PIN photodiode, with a nominal sensitive area of 7.0 mm<sup>2</sup>. The square silicon chip is housed in a colourless transparent plastic package with a thickness of 1.3 mm over the sensitive area. This plastic window was reduced to 0.7 mm in order to reduce X-ray absorption. The capacitance of the photodiode was  $(8.5 \pm 0.6)$  pF, with the reverse bias of 30 V used in the measurements. The depletion layer thickness, determined from the area and capacitance of the *p-n* junction assuming a parallel plate geometry, was

$(88 \pm 6) \mu\text{m}$ . The photodiode leads were soldered directly to a coaxial cable, with a SHV connector in the opposite end, forming a small probe 5.0 cm in length. To avoid the exposure of the photodiode to light, the probe was first covered with a  $(0.38 \pm 0.01)$  mm thick black PVC thermoshrink wrapping. This wrapping was then covered with a thin  $(3.2 \text{ mg/cm}^2)$  aluminium foil which served as an electrical shield. Some of the measurements were made without the PVC cover, but with two layers of the aluminium foil.

The electronic system utilized for the measurements consisted of an Ortec 456 HV power supply, to provide a reverse bias of 30 V to the photodiode, an Ortec 142 IH preamplifier, an Ortec 572 amplifier, a Northern NS 623 ADC, and a microcomputer adapted to operate as a multichannel analyser. All the measurements have been carried out with the photodiode and preamplifier at room temperature.

Spectra of  $X$ - and  $\gamma$ -rays emitted by the radioactive sources  $^{241}\text{Am}$ ,  $^{109}\text{Cd}$ ,  $^{133}\text{Ba}$  and  $^{152}\text{Eu}$ , with activities between  $10^4$  and  $10^5 \text{ Bq}$ , have been measured. The sources were placed at a distance of 2 cm from the photodiode. These discrete spectra were utilized to calibrate the  $X$ -ray spectrometer, which resulted in linear energy vs. channel-number curves, and to determine the energy resolution and full-energy efficiency of the photodiode. The full width at half maximum (FWHM) for the peaks of the measured source spectra, in the energy range 13–122 keV, are presented in Table I.

Continuous spectra of  $X$ -ray tubes, with electron acceleration voltages ranging from 60 to 160 kV, were obtained using the following equipment: (a) a Philips MCN 421 water cooled  $X$ -ray tube, with a tungsten target at an angle of  $30^\circ$ , 2 mm beryllium window, connected to a Philips MG 450 system with a constant potential generator stabilized within 0.3%, and 0.10 mA current in the tube; (b) a Rörix  $X$ -ray tube having a rotating tungsten/rhenium target with an angle of  $17.5^\circ$  and inherent filtration

equivalent to 1.7 mm Al, connected either to a system with a three-phase generator (with a ripple of  $\sim 10\%$ ) or to a Siemens Heliophos 4B monophasic apparatus operating in radioscopy (ripple  $\sim 2\%$ ), both with currents less than 2 mA. The focal spot-photodiode detector distance was 2.8 m for the Philips MCN 421 tube, and 1.50 m for the Rörix tube (with a Pb collimator).

## Spectral Corrections and Data Analysis

### *Photodiode efficiency for photon total energy absorption*

Commercially available PIN Si photodiodes have, in general, a small sensitive layer thickness ( $< 100 \mu\text{m}$ ), as compared to Si(Li), Ge(Li) or HP Ge detectors. Due to this thin depletion layer, the efficiency for the detection of  $X$ -ray photons presents a strong energy dependence. In the present work, the efficiency of the Siemens SFH 206K photodiode, for photon total energy absorption in diagnostic range, have been calculated and experimentally determined. As the volume of the  $i$ -layer is very small, the incident photons rarely suffer multiple interactions (less than 1% of the total). Then we may assume that the total energy photon absorption in Si occurs only by photoelectric effect, and the partial absorption only by Compton scattering.

The efficiency for the photoelectric effect may be calculated by

$$\eta_p = (\mu_p/\mu_t) \left(1 - e^{-\frac{\mu_t}{\rho}t}\right) \quad (1)$$

where  $\mu_p$  and  $\mu_t$  are the photoelectric and total linear attenuation coefficients for Si in  $\text{cm}^{-1}$ , respectively (Storm and Israel, 1970),  $\rho$  is the Si density in  $\text{g/cm}^3$  and  $t$  is the depletion layer thickness (in  $\text{g/cm}^2$ ). The  $K$ -escape may be also ignored in this case due to the low energy of the  $K$ -edge for Si (1.84 keV) and the low probability for

fluorescence (0.05). On the other side, for a Si photodiode, the escape of photoelectrons must be considered, since the extrapolated range of 100 keV electrons in silicon is 58  $\mu\text{m}$ , very close to the thickness of the depletion layer of 88  $\mu\text{m}$ . The data presented by Aoki and Koyama (Aoki and Koyama, 1989) have been utilized for the determination of the fraction  $f_e$  of photoelectrons that escape from the silicon  $i$ -layer, after the photon interaction. In this determination, only the frontal scattering probability of the photoelectrons, after a photon interaction with a Si atom, is considered. The efficiency for total energy absorption, corrected for the escape of photoelectrons, will then be given by

$$\eta_f = \eta_p (1 - f_e) \quad (2)$$

For the measurements carried out in the present work, it was still necessary to correct  $\eta_f$  for the attenuation of the photon beam in the materials between the X-ray source and the sensitive layer of the photodiode, namely: the dead Si  $p^+$  layer ( $\leq 1 \mu\text{m}$ ) (Sakai, 1987; Gramsch et al., 1992), the photodiode plastic wrapping, the black PVC thermoschrink wrapping, the Al foil electrical shield, and air. Thus, the efficiency  $\eta'_f$  corrected for the attenuation in these materials is given by

$$\eta'_f = \eta_f \cdot f_d \quad (3)$$

where  $f_d$  is the product of the absorption factors related to each one of the considered materials.

The calculated efficiency  $\eta'_f$ , using equation 3, for several energies of X- and  $\gamma$ -rays emitted by  $^{109}\text{Cd}$ ,  $^{133}\text{Ba}$ , and  $^{152}\text{Eu}$ , sources are presented in Table II. Also shown are experimental data obtained from the ratio of measured full-energy peak counting rates to the respective published emission rates (Rens and Westmeier, 1983), after correction of these last rates for the absorption in the radioactive source covers. The experimental efficiencies  $\eta_{f,\text{exp}}$  are normalized to the calculated  $\eta'_f$  values at 88.034 keV (for  $^{109}\text{Cd}$ ),

30.625/30.973 keV (for  $^{133}\text{Ba}$ ), and 121.77 keV (for  $^{152}\text{Eu}$ ). Figure 1 shows  $\eta'_f$  and  $\eta_{f,\text{exp}}$  versus photon energy in the energy range covered in the present work.

#### *Correction (Stripping) of the Experimental Obtained Spectra*

In order to correct the experimental data to obtain the original radiation spectrum, a microcomputer program (Stripping 2.0) has been developed in Mathcad (Mathsoft, Inc.). Such program takes into account the efficiency for total energy absorption, the Compton scattering, the radiation scattered by the metallic components of the photodiode, and the attenuation of the incident beam by the materials located between the radiation source and the sensitive region of the detector. A flowchart of this program is presented in the Appendix.

After the reading of the files containing the experimental data corresponding to measurements with and without the radiation source (noise), the program initiates the net counting correction starting from the last channel. The measured data are then corrected for the photodiode efficiency, calculated by equation 3 and presented in Table II and Figure 1.

Values for the attenuation coefficients of Si and materials between the radiation source and the sensitive layer of the photodiode have been calculated using a least square fit to the data obtained in the literature (Storm and Israel, 1970; Hubbel, 1982).

The distortion due to Compton scattering is corrected by assuming a rectangular shape approximation for the scattered spectrum below the Compton-edge (Aoki and Koyama, 1989; Seelentag and Panzer, 1979). The efficiency for Compton scattering is given by

$$\eta_c = (\mu_c/\mu_t) \left(1 - e^{-\frac{\mu_t}{\rho} t}\right) \quad (4)$$

where  $\mu_c$  and  $\mu_t$  are the linear attenuation coefficients in Si for Compton scattering and total energy absorption, respectively,  $\rho$  is the Si density and  $t$  is the thickness of the depletion region. It is not necessary to take into account the escape of the recoil electrons, since their range in silicon is much smaller than the depletion layer ( $\sim 6 \mu\text{m}$  for 28 keV electrons produced by 100 keV photons). For the correction, the average counting per channel in the Compton continuum  $h$  (the rectangle height) is finally subtracted in the region from channel 1 to channel  $c$ , corresponding to the Compton-edge. This average counting  $h$  may be determined by the expression

$$hc = \eta_c N_T \quad (5)$$

where  $\eta_c$  is the efficiency for Compton scattering given by equation 4, and  $N_T$  is the corrected counting in the peak corresponding to the total energy of related photons. Such a procedure is carried out channel by channel, beginning also in the last and ending in the first channel.

There is also the necessity to correct the measured spectra for the radiation scattered by the metallic components of the photodiode. The Si wafer of the Siemens SFH 206K photodiode is mounted on a metallic contact of silver and indium. Such metallic layer may scatter photons that did not interact with the depletion layer of the Si wafer. For instance, the photons backscattered at  $180^\circ$  by Compton effect, occurred with 59.5 keV incident photons from  $^{241}\text{Am}$ , have an energy of 48.2 keV. Photoelectrons which escape from this metallic contact may also reach the sensitive layer of the Si wafer. In our case, the experimental data were corrected for the scattered radiation by utilizing counts obtained with spectra of the radioactive sources  $^{241}\text{Am}$ ,  $^{133}\text{Ba}$ , and  $^{109}\text{Cd}$ , respectively between the isolated peaks of 59.54, 80.99, and 88.03 keV, and the peaks immediately lower in energy, for each case. For the respective correction, such counts were supposed to be constant from zero to the channel corresponding to the

energy of the photons that have caused the scattered radiation. The ratio  $F$  of the integral of the "scattered" counts to the integral of the photoelectric peak counts is energy dependent; such dependence has been determined by a linear regression of the values obtained from a curve of  $F$  as a function of the photon energy. The fraction  $F$  of the "scattered" counts is then subtracted from the measured counts in each channel.

Besides the radiation scattered by the metallic contact, photoelectric processes occurred in Ag and In will produce secondary (fluorescence) X-rays that will also be detected in the Si depletion layer, resulting in an additional spectrum superposed on the spectrum of interest. The characteristic  $K$  X-rays of silver have energies of 21.99, 22.16, 24.93, and 25.43 keV, and those of indium 24.21, 27.27, and 27.86 keV. The correction taking into account these fluorescence X-rays is particularly difficult. Other photodiodes will need or not this correction, depending on the fabrication process. In the present work, the correction for the Ag characteristic  $K$  X-rays, the major contribution to this fluorescence, has been carried out by utilizing the spectrum of the  $^{109}\text{Cd}$  source, previously measured; this nuclide decays to an isotope of Ag which emits its characteristic X-rays. Such Ag characteristic X-ray spectrum may be normalized to and subtracted from the measured data.

#### Calculation of Semi-Empirical Spectra Based on TBC Model

The model proposed by Tucker et al. (TBC model) (Tucker, Barnes and Chakraborty, 1991) presents different formulations for the evaluation of both continuum spectra (*Bremsstrahlung*) and characteristic lines emitted by an X-ray tube. The model considers the target material and attenuation, the geometry of the anode and the attenuation by the tube window and added filtration. The proposed equation for the

Bremsstrahlung was

$$N(E)dE = \frac{\alpha \cdot r_e^2 \cdot Z^2}{A} \frac{dE}{E} \int_E^{T_0} \frac{B(T + m_0 c^2)}{T} F(E, T) \cdot \left( \frac{1}{\rho} \frac{dT}{dx} \right)^{-1} dT \quad (6)$$

where:  $\alpha$  is the fine structure constant;  $r_e$  is the classical electron radius;  $m_0$  is the rest mass of the electron;  $c$  is the velocity of light;  $Z$  and  $A$  are the effective atomic number and the mass of the target atoms respectively;  $T_0$  is the initial kinetic energy of the electrons;  $T$  is the kinetic energy of the electrons inside the target;  $(1/\rho)(dT/dx)$  is the mass stopping power of the target atoms;  $B$  is a function proportional to the number of X-ray photons emitted per electron, and

$$\begin{aligned} F(E, T) &= \exp[-\mu_{WR}(E) \cdot d] = \exp[-\mu_{WR}(E) \cdot x/\text{sen}\theta] = \\ &= \exp[-\mu_{WR}(E) \cdot (T_0^2 - T^2) / (\rho C \text{sen}\theta)] \end{aligned} \quad (7)$$

where:  $\mu_{WR}(E)$  is the linear attenuation coefficient of the target material for an X-ray of energy  $E$ ;  $\theta$  is the target angle; and  $C = (T_0^2 - T^2)/\rho x$  is the Thomson-Widdington constant.

The model considers a parabolic probability distribution function in order to account for the characteristic emission by the target material. This distribution appears as a function of the distance  $x$  travelled by the electrons inside the anode and was modeled as

$$P\left(\frac{x}{R}\right) = \begin{cases} \cdot \left(\frac{3}{2}\right) \left[1 - \left(\frac{x}{R}\right)^2\right], & x \leq R \\ \cdot 0, & x > R \end{cases} \quad (8)$$

where  $R$  is the distance at which the average kinetic energy of the electrons is equal to the K-shell binding energy. By using this function, the characteristic emission can be calculated by

$$N(E_i) = A_k \left(\frac{T_0}{E_k} - 1\right)^{n_k} f(E_i) \int_0^R P\left(\frac{x}{R}\right) e^{-\mu_{WR}(E_i)x/\text{sen}\theta} dx \quad (9)$$

where  $A_k$  and  $n_k$  are model parameters and  $f(E_i)$  is the fractional emission for the characteristic energy  $E_i$ .

A routine for implementing the equations above were developed also by using the Mathcad software. Both model parameters and parametrized equations for the mass stopping power and for the function  $B$  followed the indications included in the Tucker et al. paper. Values of the Thomson-Widdington constant were provided for electron incident energies of 50, 75, 100, 150 and 200 keV. This values were interpolated by using the spline fitting routine included in the Mathcad package, in order to provide a continuous grid for calculating the X-ray spectra. Results of a computer simulation of 60, 73, 100 and 160 kVp spectra by using this methodology are presented in Figures 4 to 7.

## Results and Discussion

Results of the measurements of X- and  $\gamma$ -ray spectra using a Siemens SFH 206K photodiode, in the energy range 15–160 keV, are presented in Figures 2 to 7. The raw data have been corrected by the procedure described previously.

The measured and corrected spectra of  $^{241}\text{Am}$  and  $^{133}\text{Ba}$  are presented in Figures 2 and 3, respectively; the circles are experimental data and the solid lines have been drawn just to guide the eye. The values for the full width at half maximum (FWHM) of the peaks are presented in Table I. The relative intensities of peaks in the measured photon spectra have been determined and compared with corresponding data published in the literature (Browne and Firestone, 1986). The result of this comparison is presented in Table III, showing a good agreement.

The measured and corrected spectra of beams emitted by X-ray tubes are presented in Figures 4 to 7. Figure 4(a) presents the measured spectrum (raw data) for

the beam of the Philips MCN 421 tube described previously, with a constant potential of 160 kV, current of 0.10 mA, and an additional filtration of 4.0 mm Al and 0.5 mm Cu. The corrected spectrum corresponding to the one shown in Figure 4(a) is presented in Figure 4(b). In this figure, the circles are the corrected experimental data and the solid line corresponds to the calculated spectrum on the basis of the TBC model. The experimental and theoretical data were normalized in the maximum of the Bremsstrahlung (continuous) spectrum. The peaks at 59.3 keV and 67.2 keV, observed in Figures 4(a)(b), correspond to the characteristic *X*-rays of the tungsten target. The agreement between the experimental and theoretical results is good for the continuous part of the spectrum. In the characteristic *X*-rays region, the agreement is not so good due to the different resolutions of the experimental and theoretical data. The broadening of the characteristic *X*-rays peaks in the theoretical spectrum is due to the choice of the resolution in the energy scale used in the calculation.

Figures 5 to 7 present the comparison of the corrected experimental and theoretical (TBC model) spectra related to the beam of the Rörix *X*-ray tube described previously. The conditions were as follows: Figure 5 — applied voltage of 60 kV, as supplied by the Heliophos 4B monophase apparatus operating in radioscopy (ripple  $\sim 2\%$ ), current  $\sim 2$  mA, and an additional filtration of 3.4 mm Al and 0.6 mm Cu; Figure 6 — applied voltage of 73 kV, as supplied by the same monophase generator as in Figure 5, and an additional filtration of 1.2 mm Al; Figure 7 — applied voltage of 100 kV by the already described three-phase generator system, current  $\sim 2$  mA, additional filtration of 4.7 mm Al.

The agreement between the experimental and theoretical spectra for the Rörix tube is reasonable but not so good as the one observed for the Philips MCN 421 tube. This is possibly due to the fact that the theoretical spectra have been calculated assuming

a constant potential, and the Rörix tube has been operated with potentials with a percentage ripple greater than zero.

The present work has demonstrated that a simple detector, as a low cost photodiode at room temperature, is adequate for the measurement of *X*-ray tube spectra. The resolution of these detectors (3–4 keV) is sufficient to characterize the *X*-ray beams, whose spectra are dominated by the continuous bremsstrahlung component. The comparison with calculated spectra supports this conclusion.

#### Acknowledgements

We would like to thank Dr. Marília Teixeira da Cruz for her assistance in the measurements with the Philips *X*-ray tube, and Mr. Victor E.J. São Vicente for his help in developing the stripping program.



Table I — Full width at half maximum (FWHM) of the peaks obtained in the spectral measurements with radioactive sources.

Source	Peak energy (keV)*	FWHM (keV)
<sup>241</sup> Am	13.927	3.4
<sup>241</sup> Am	17.611	3.4
<sup>109</sup> Cd	22.163	3.9
<sup>241</sup> Am	26.344	2.5
<sup>133</sup> Ba	30.973	4.1
<sup>152</sup> Eu	40.118	4.1
<sup>133</sup> Ba	53.148	2.9
<sup>241</sup> Am	59.536	4.0
<sup>133</sup> Ba	80.989	4.0
<sup>109</sup> Cd	88.034	3.6
<sup>152</sup> Eu	121.776	4.2

Table II — Efficiency  $\eta'_f$ , as calculated by equation (3) and normalized experimental data  $\eta_{f,exp}$  (see text).

Source	Energy (keV)	$\eta'_f$	$\eta_{f,exp}$
<sup>109</sup> Cd	21.990/22.163	$4.32 \times 10^{-2}$	$(4.75 \pm 0.25) \times 10^{-2}$
	24.934/25.603	$3.08 \times 10^{-2}$	$(3.34 \pm 0.19) \times 10^{-2}$
	88.034	$6.30 \times 10^{-4}$	$6.30 \times 10^{-4}$
<sup>133</sup> Ba	30.625/30.973	$1.84 \times 10^{-2}$	$1.84 \times 10^{-2}$
	34.967/36.006	$1.25 \times 10^{-2}$	$(1.11 \pm 0.02) \times 10^{-2}$
	53.148	$3.38 \times 10^{-3}$	$(2.76 \pm 0.57) \times 10^{-3}$
<sup>152</sup> Eu	79.612/80.989	$8.52 \times 10^{-4}$	$(8.93 \pm 0.54) \times 10^{-4}$
	39.522/40.118	$8.42 \times 10^{-3}$	$(8.0 \pm 2.6) \times 10^{-3}$
	45.379/46.819	$5.53 \times 10^{-3}$	$(5.7 \pm 1.9) \times 10^{-3}$
	121.77	$1.93 \times 10^{-4}$	$1.93 \times 10^{-4}$

\*Browne and Firestone, 1986.

Table III — Ratios of peak intensities  $R$ , obtained from the measured radioactive source photon spectra (after stripping), as compared to the corresponding ratios  $RL$  taken from the literature, for  $^{241}\text{Am}$  and  $^{133}\text{Ba}$ .

Source	$A_1$	$A_2$	$R = \frac{A_1}{A_2}$	$RL$
$^{241}\text{Am}$	$6.468 \times 10^4$ counts (26.3 keV)	$1.138 \times 10^6$ counts (59.54 keV)	0.057	0.056
$^{133}\text{Ba}$	$2.811 \times 10^7$ counts (30.625/30.973+ 34.967/36.006) keV	$9.340 \times 10^6$ counts (79.612/80.989) keV	3.01	2.97

$A_1$ : area under the first peak (counts).

$A_2$ : area under the second peak (counts).

$R = A_1/A_2$ : ratio of the peak intensities (areas), after stripping.

$RL$ : ratio of the peak intensities taken from the literature (Browne and Firestone, 1986), corrected for absorption in the source covers (0.22 mm of polyethylene + 0.52 mm of Al).

## REFERENCES

- Ahmad I. and Wagner F. (1979) A simple cooled Si(Li) electron spectrometer. *Nucl. Instrum. Meth.* **116**, 465-469.
- Ahmad I., Betts R.R., Happ T., Henderson D.J., Wolfs F.L.H. and Wuosman A.H. (1990) Nuclear spectroscopy with Si PIN diode detectors at room temperature. *Nucl. Instr. Meth.* **A299**, 201-204.
- Aoki K. and Koyama M. (1989) Measurement of diagnostic X-ray spectra using a silicon photodiode. *Med. Phys.* **16**, 529-536.
- Aoki K. and Koyama, M. (1990) A silicon diode in a thimble-type mount for measurement of diagnostic X-ray spectra. *Phys. Med. Biol.* **35**, 105-1517.
- Browne E. and Firestone R.B. (1986) Table of radioactive isotopes, Shirley V. (ed.), John Wiley & Sons.
- Epp E.R. and Weiss H. (1966) Experimental study of photon energy spectrum of primary diagnostic X-rays. *Phys. Med. Biol.* **11**, 225-238.
- Fewell T.R. and Shuping R.E. (1977) Photon energy distribution of some typical diagnostic X-ray beams. *Med. Phys.* **4**, 187-197.
- Gramsch E., Lynn K.G., Weber M., DeChillo B. and Mc Williams J.R. (1992) Silicon PIN photodetectors in high resolution nuclear spectroscopy. *Nucl. Instr. Meth.* **A311**, 529-538.
- Hubbel J.H. (1982) Photon mass attenuation and energy-absorption coefficients from 1 keV to 20 MeV. *Int. J. Appl. Radiat. Isot.* **33**, 1269-1290.
- Israel H.I., Lier D.W. and Storm E. (1971) Comparison of detectors used in measurements of 10 to 300 keV X-ray spectra. *Nucl. Instr. Meth.* **91**, 141-157.

## FIGURE CAPTIONS

Figure 1— Full-energy absorption efficiency  $\eta'_f$  and  $\eta_{f,\text{exp}}$  versus photon energy for the SFH 206K photodiode. The solid line represents the calculated  $\eta'_f$  and the circles with error bars correspond to the experimental  $\eta_{f,\text{exp}}$  data of Table II. Error bars are related only to the least square fits to the spectral peaks.

Figure 2— (a) Measured X- and  $\gamma$ -ray spectrum of  $^{241}\text{Am}$ . (b) Corrected X- and  $\gamma$ -ray spectrum of  $^{241}\text{Am}$ .

Figure 3— (a) Measured X- and  $\gamma$ -ray spectrum of  $^{133}\text{Ba}$ . (b) Corrected X- and  $\gamma$ -ray spectrum of  $^{133}\text{Ba}$ .

Figure 4— (a) Measured X-ray spectrum of the beam emitted by the Philips MCN 421 tube (constant potential of 160 kV). (b) Comparison of the corrected experimental spectrum of (a) (circles) with the TBC model calculated spectrum (solid line). The data have been normalized at the maximum of the Bremsstrahlung spectrum (see text for details).

Figure 5— Comparison of the corrected experimental (circles) and theoretical - TBC model (solid curve) spectra of the beam emitted by the Rörlix X-ray tube; applied voltage of 60 kV (monophase generator, radiology regime  $\sim 2\%$  ripple) (see text for details).

Figure 6— Same as Figure 5, for an applied voltage of 73 keV (see text for details).

Figure 7— Same as Figure 5, for an applied voltage of 100 kV by a three-phase generator (ripple  $\sim 10\%$ ) (see text for details).

O'Foghludha F. and Johnson G.A. (1981) Voltage wave forms effects on output and penetration of W - and  $M_0$  - anode mammographic tubes. *Phys. Med. Biol.* **26**, 291-303.

Pani R., Laitano R.F. and Pellegrini R. (1987) Diagnostic X-ray spectra measurements using a silicon surface barrier detector. *Phys. Med. Biol.* **32**, 1135-1149.

Rens V. and Westneier W. (1983) Catalog of  $\gamma$ -rays from radioactive decay, Part II. *Atomic and Nucl. Data Tables* **29**, 193-406.

Sakai E. (1987) Recent measurements of scintillator-photo detectors systems. *IEEE Trans. Nucl. Sci.* **NS-34**, 418-422.

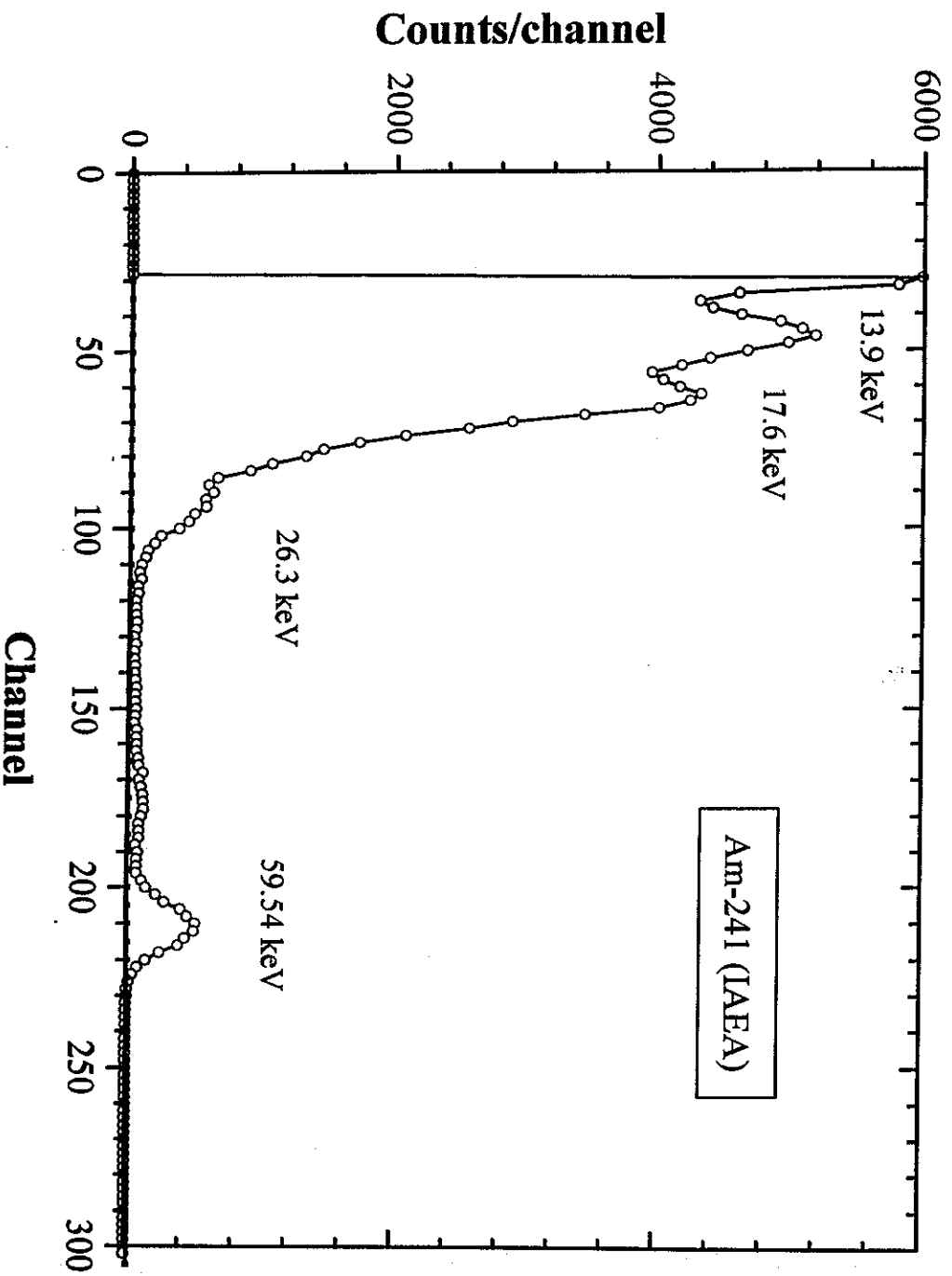
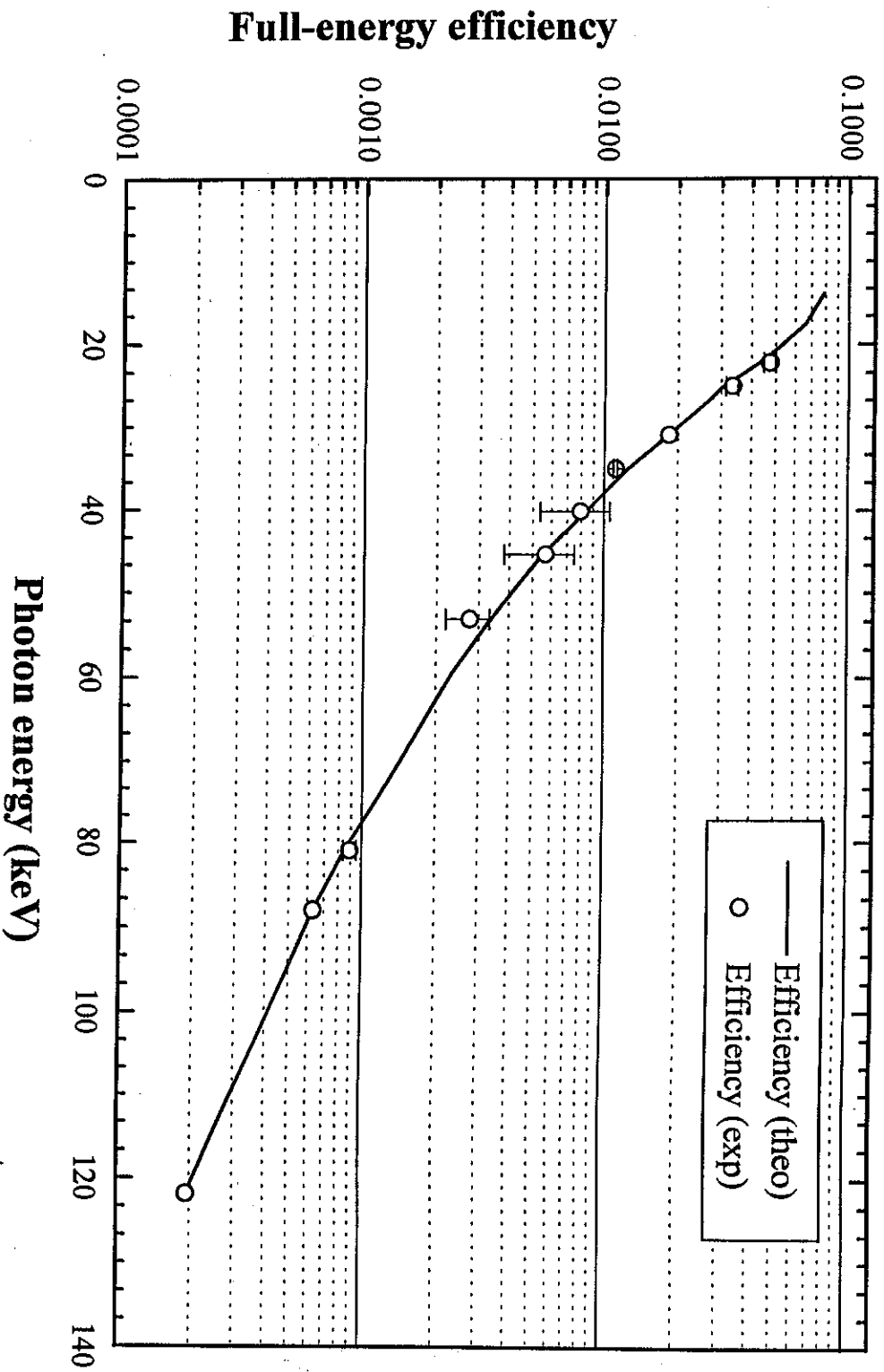
Seelentag W.W and Panzer W. (1979) Stripping of X-ray bremsstrahlung spectra up to 300 kVp on a desk type computer. *Phys. Med. Biol.* **24**, 767-780.

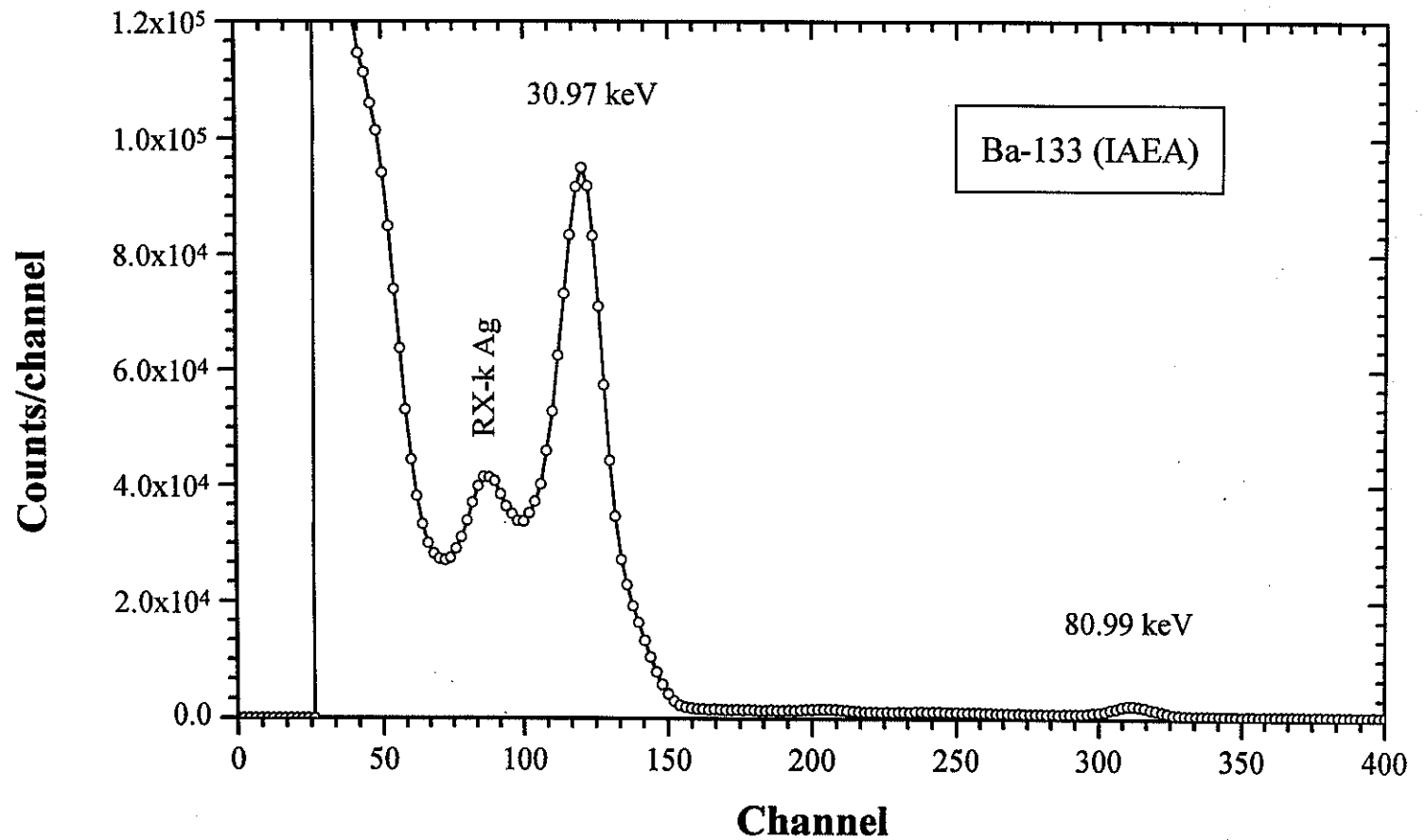
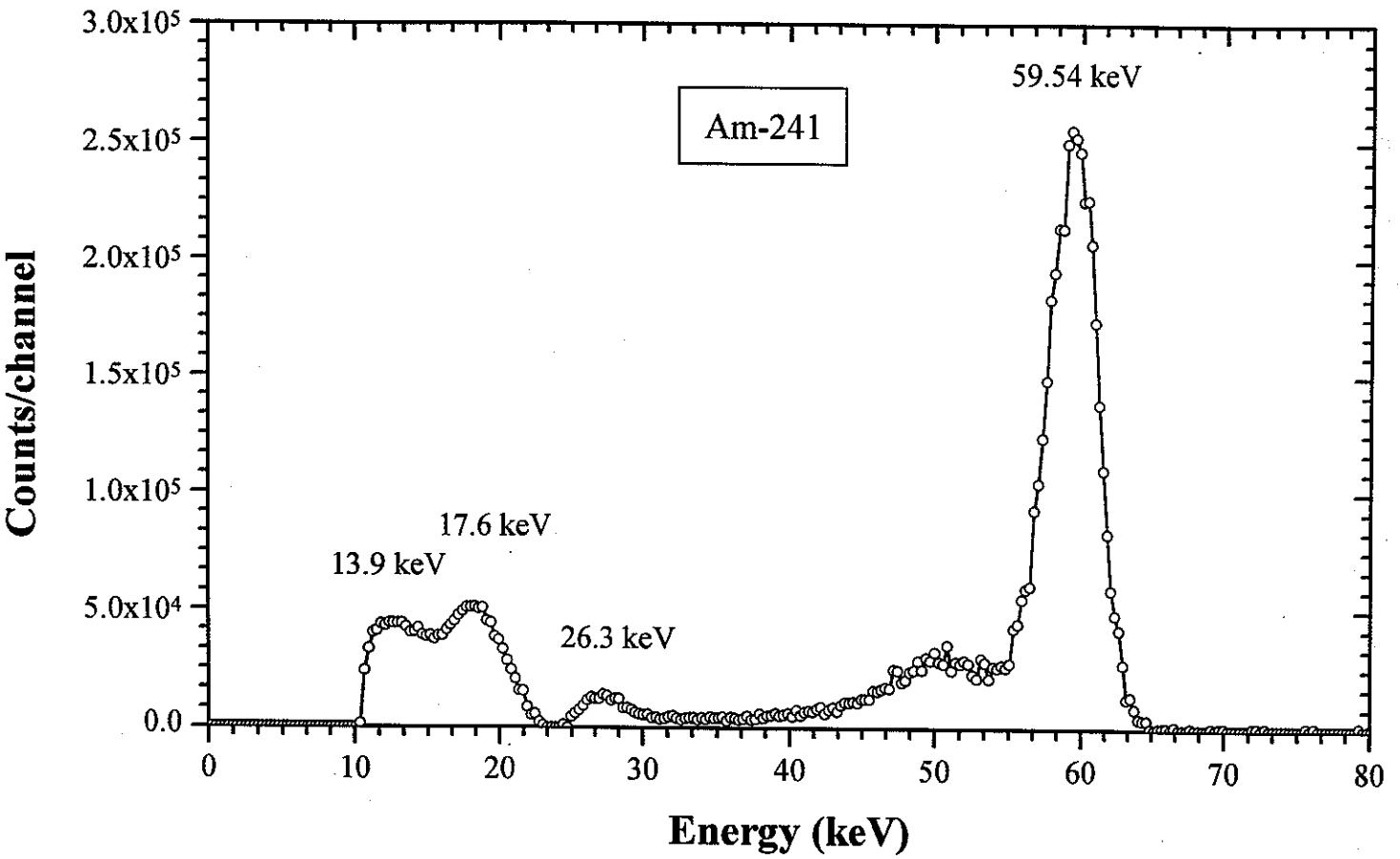
Storm E. and Israel, H.I. (1970) Photon cross sections from 1 keV to 100 MeV for elements  $Z = 1$  to  $Z = 100$ . *Nucl. Data Tables* **A7**, 565-681.

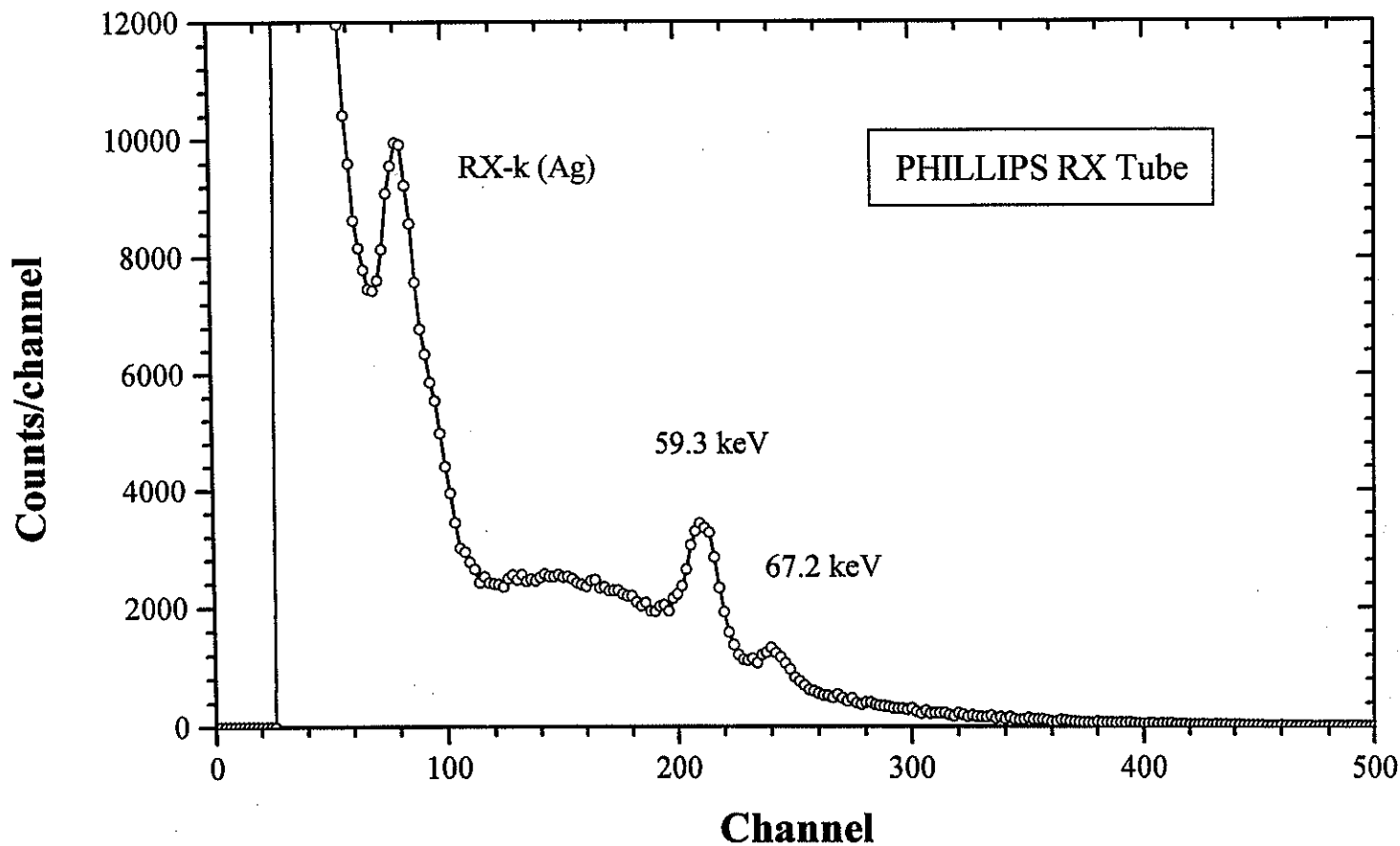
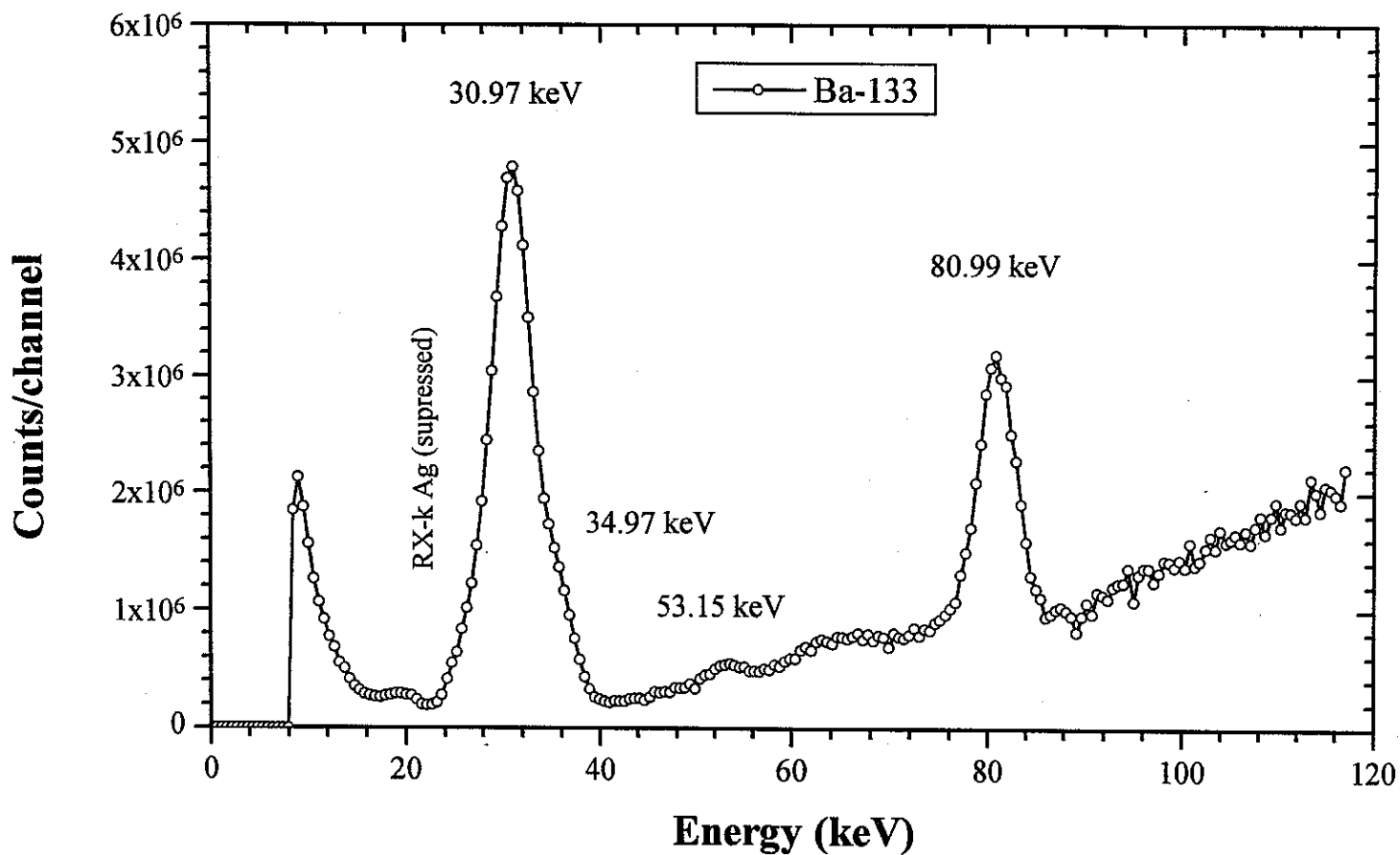
Suffert M. (1992) Silicon photodiode readout of scintillators and associated electronics. *Nucl. Instr. Meth.* **A322**, 532-528.

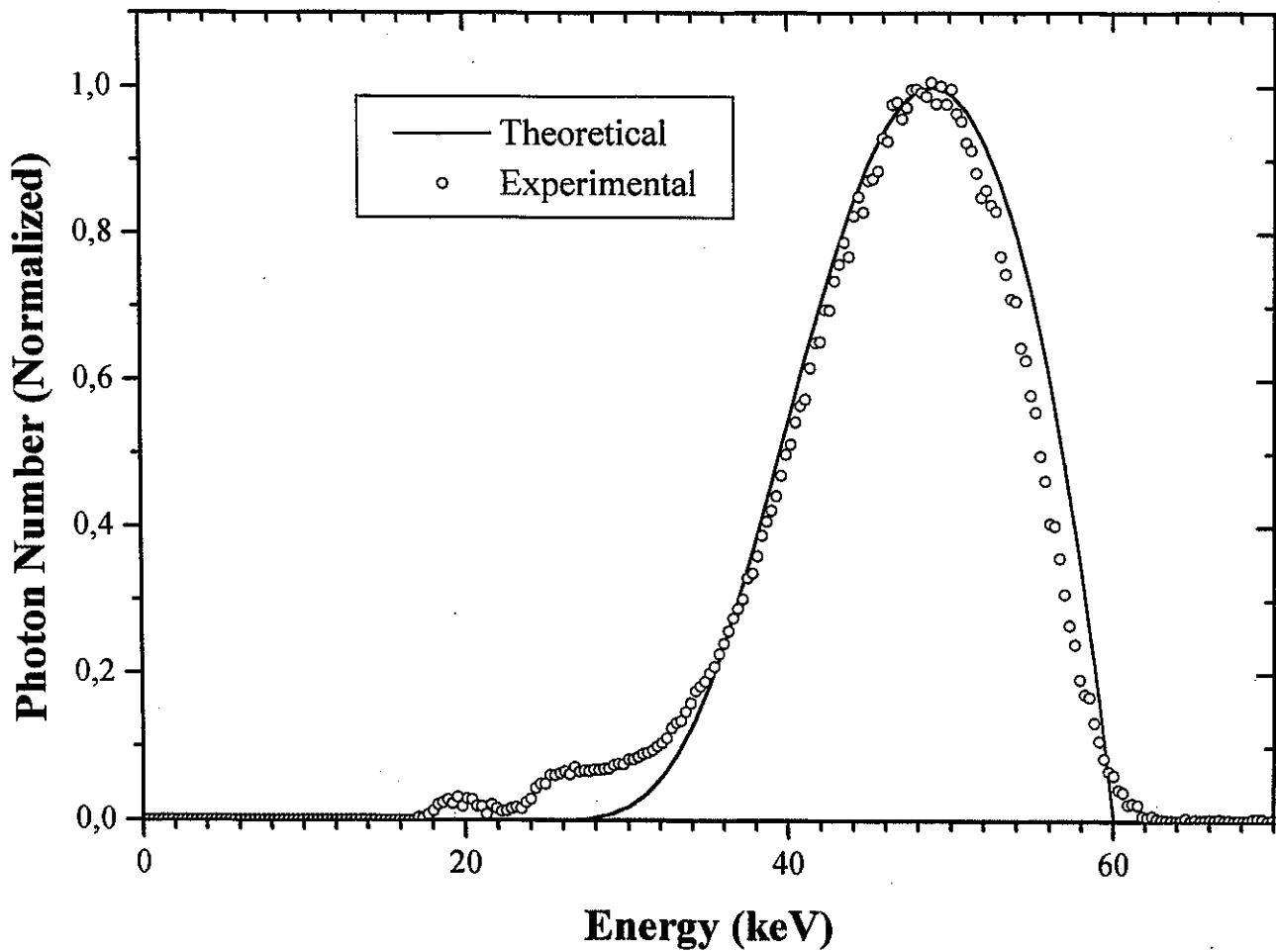
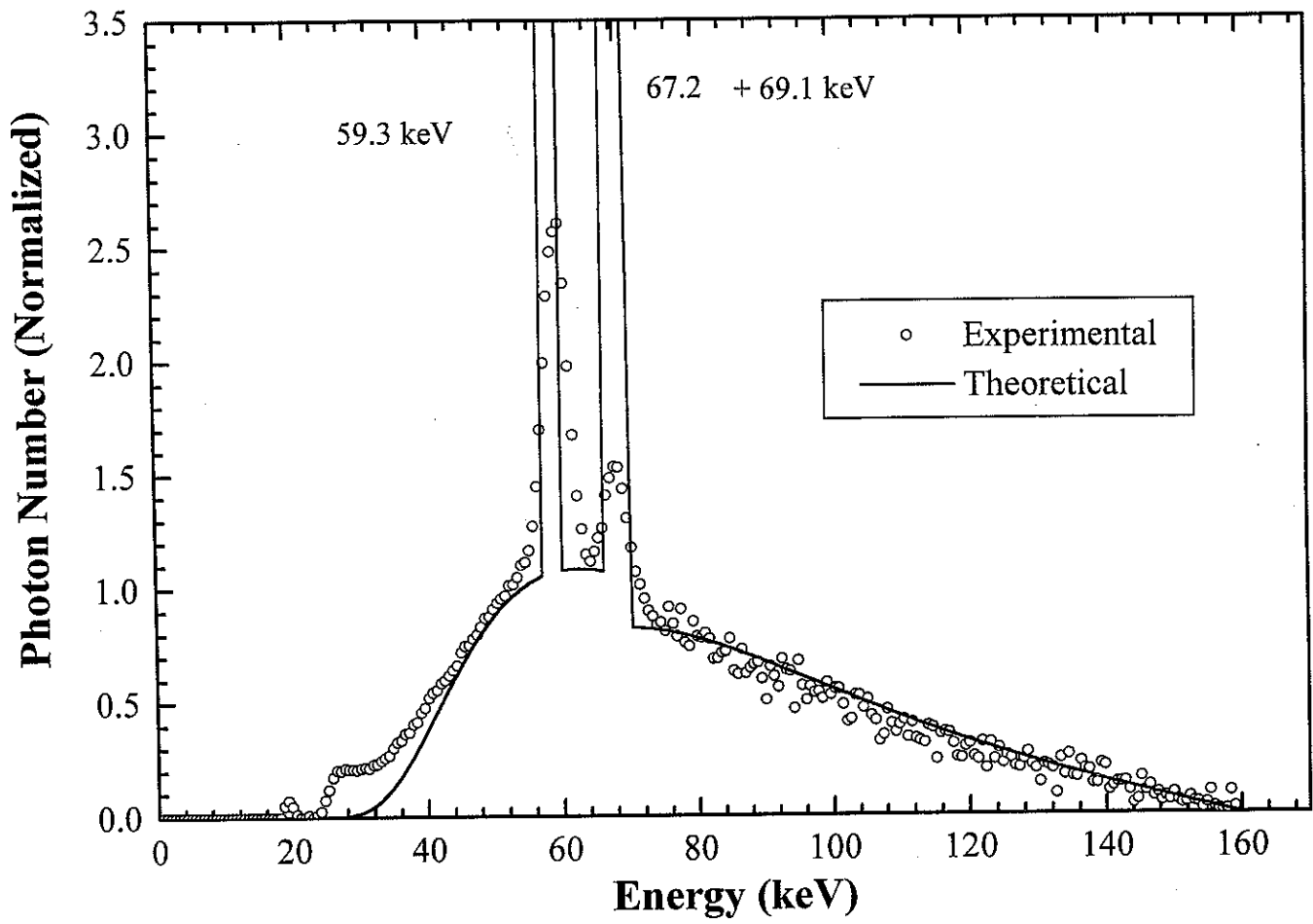
Tucker D.M., Barnes G.T. and Chakraborty D.P. (1991) Semiempirical model for generating tungsten target X-ray spectra. *Med. Phys.* **18**, 211-218.

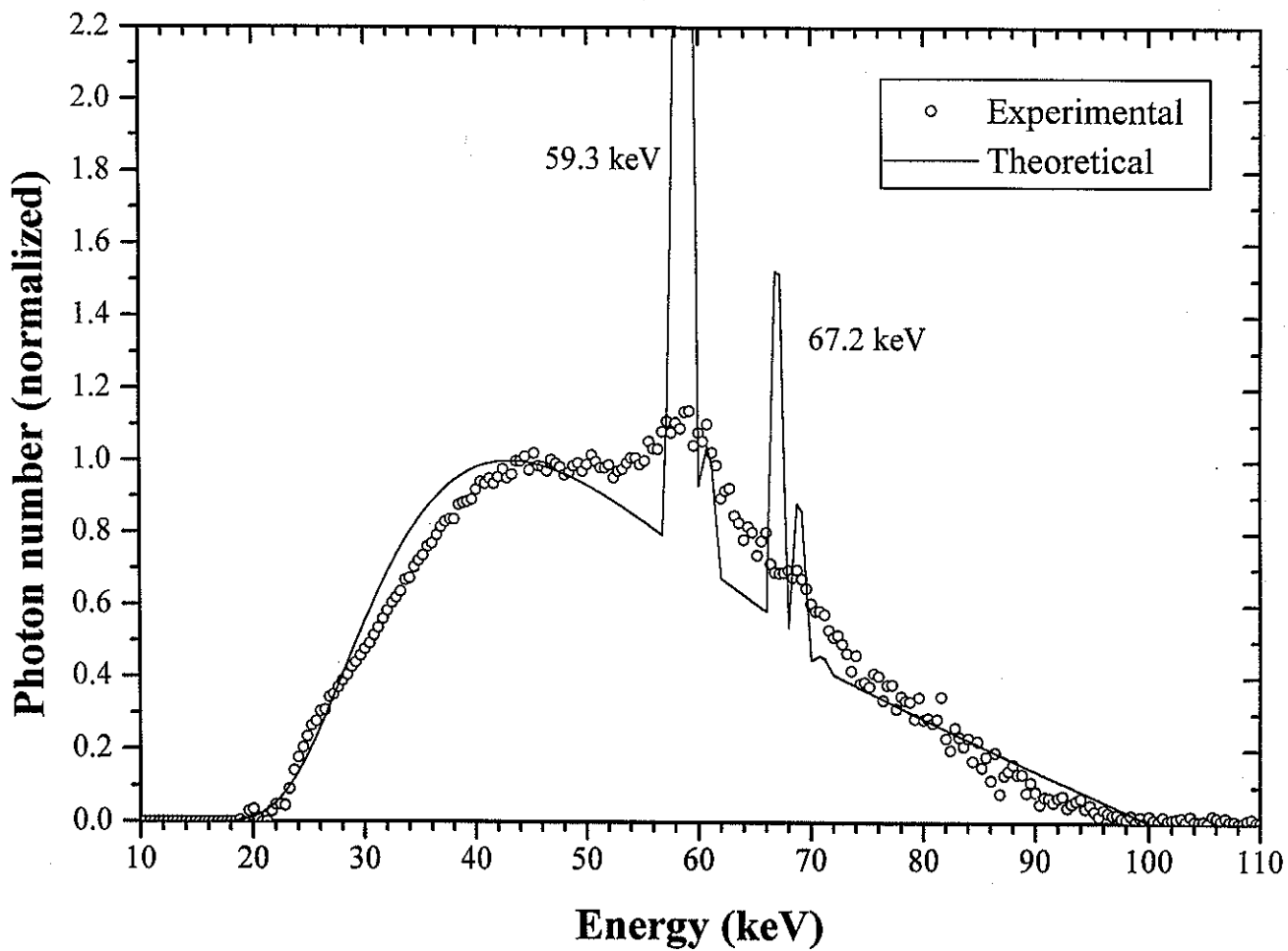
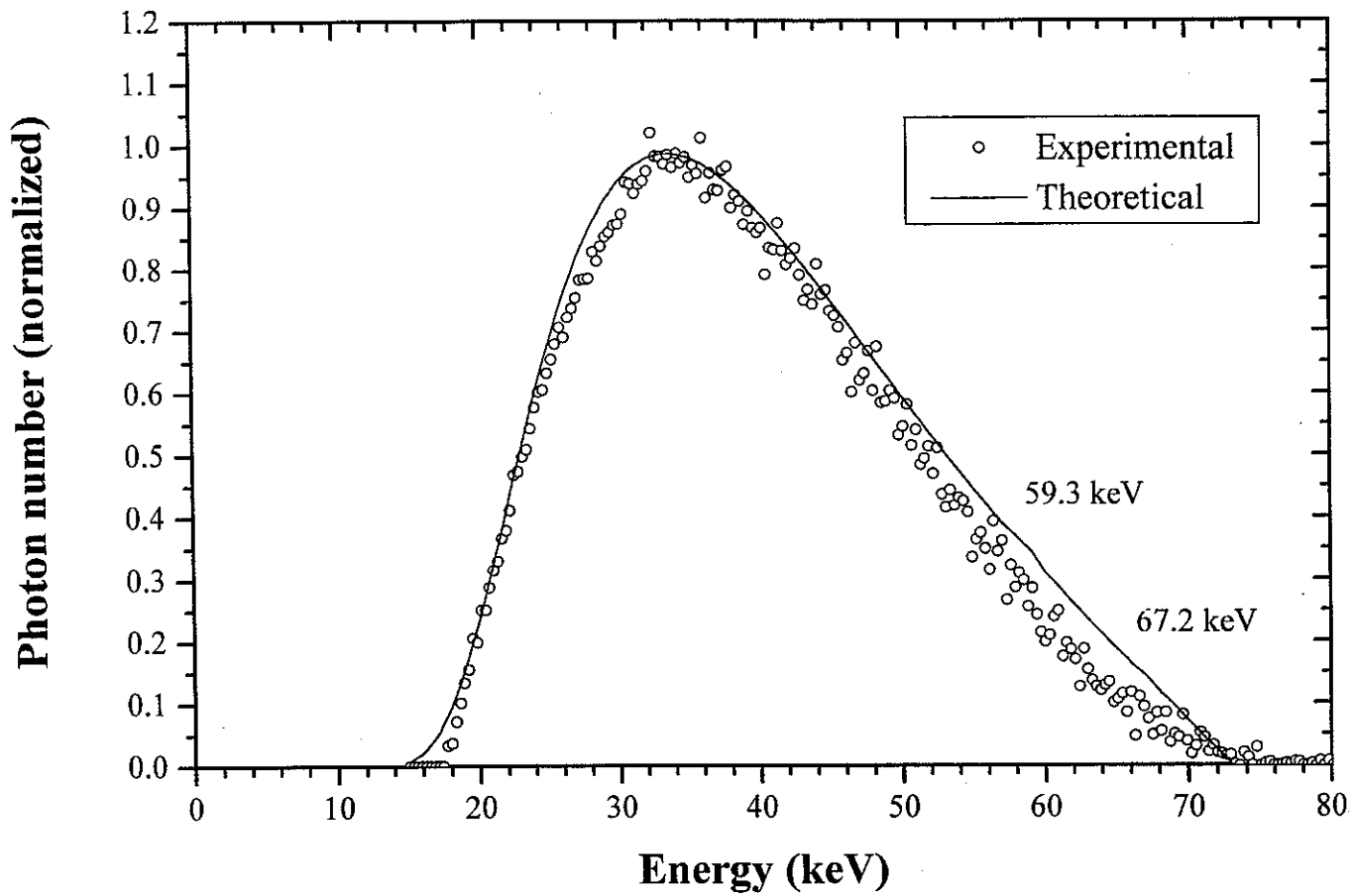
Yamamoto H., Hatakeyama S. Norimura T. and Tsuchiya T. (1989) Low-energy nuclear radiation detection with a silicon photodiode. *Nucl. Inst. Meth.* **A281**, 128-132.













**FLOW CHART OF PROGRAM FOR THE STRIPPING OF  $\gamma$ - AND X-RAYS  
SPECTRA MEASURED WITH PIN PHOTODIODE.**

